

3D Shape Retrieval via Irrelevance Filtering and Similarity Ranking (IF/SR)

Xiaqing Pan, Yueru Chen, C.-C. Jay Kuo

Ming-Hsieh Department of Electrical Engineering, University of Southern California,
Los Angeles, CA 90089-2564, USA

Abstract. A novel solution for the content-based 3D shape retrieval problem using an unsupervised clustering approach, which does not need any label information of 3D shapes, is presented in this work. The proposed shape retrieval system consists of two modules in cascade: the irrelevance filtering (IF) module and the similarity ranking (SR) module. The IF module attempts to cluster gallery shapes that are similar to each other by examining global and local features simultaneously. However, shapes that are close in the local feature space can be distant in the global feature space, and vice versa. To resolve this issue, we propose a joint cost function that strikes a balance between two distances. Irrelevant samples that are close in the local feature space but distant in the global feature space can be removed in this stage. The remaining gallery samples are ranked in the SR module using the local feature. The superior performance of the proposed IF/SR method is demonstrated by extensive experiments conducted on the popular SHREC12 dataset.

1 Introduction

Content-based 3D shape retrieval [1] has received a lot of attention in recent years due to an rapidly increasing number of 3D models over the Internet (e.g., Google sketchup and Yobi3D). Applications of 3D shape retrieval technologies include: 3D model repository management, mechanical components retrieval, medical organ model analysis, etc. Given a 3D shape model as the query, a content-based 3D shape retrieval system analyzes the query shape and retrieves ranked 3D shapes from the gallery set according to a similarity measure. Its performance is evaluated by consistency between ranked shapes and human interpretation. A robust and efficient 3D shape retrieval system is needed for users to access and exploit large 3D datasets effectively.

Recently, convolutional neural-network (CNN) based solutions achieved impressive performance by training a network using either multiple views of 3D shapes [2,3,4,5,6] or the 3D volumetric data [7,8,9]. However, their training procedure demands a large amount of labeled data, which is labor-intensive. In this work, we address the 3D shape retrieval problem using an unsupervised learning approach. It has broader applications since no labeled data are needed.

The main challenge in 3D shape retrieval lies in a wide range of shape variations. A generic 3D shape dataset such as SHREC12 [10] includes both rigid

and non-rigid shapes. Shape variations can be categorized into inter-class similarities and intra-class variations. For the latter, we have articulation, surface deformation, noise, etc.

Global and/or local features can be used to measure the similarity between two 3D shapes. The rotation invariant spherical harmonics (RISH) [11] and the D2 shape distribution [12] are two representative global features. They capture object surface properties using the frequency decomposition and the vertex distance histogram, respectively. The retrieval performance using global features only may degrade due to the loss of fine shape details. To overcome this limitation, research efforts in recent years have focused on developing more discriminative local features. They can be categorized into surface-based and view-based features. Surface-based local features [13,14,15,16,17] describe a local surface region to achieve pose oblivion, scale and orientation invariance. Although surface-based retrieval methods are effective in handling non-rigid shape retrieval [18,19], they are not robust against shape artifacts that do occur in generic shape datasets. Retrieval methods using view-based local features are favored for this reason.

View-based methods project a 3D shape into multiple views. Generally speaking, an adequate number of view samples can represent a 3D shape well. The light field descriptor (LFD) method [20] and the multi-view depth line approach (MDLA) [21] represent each view by Zernike moments plus polar Fourier descriptors and depth lines, respectively. The similarity between two shapes is measured by enumerating multiple rotation setups. The salient local visual feature (SLVF) method [22] extracts the SIFT points [23] from each range view. After constructing a codebook from the training pool, one feature of a 3D shape can be represented by the histogram of SIFT points from all views using the Bag of Words (BoW) approach. The DG1SIFT method [24] extends the SLVF method by extracting three types of SIFT points from each view. They are dense, global and one SIFTs. The depth buffered super vector coding (DBSVC) method [25] uses a dense power SURF feature and the super vector coding algorithm to improve the feature discriminability.

Although local features achieve a better performance than global features when being tested against several generic 3D shape datasets [10,26,27,28], their discriminative power is restricted in the global scale. In particular, they may retrieve globally irrelevant 3D shapes in high ranks. To illustrate this point, we show five retrieval results by applying the DG1SIFT method to the SHREC12 3D shape dataset in Fig. 1 (a)-(e). With the five query shapes in the leftmost column, the top 10 retrieved results are presented in the first row of each subfigure. Obviously, errors in these retrieval results are counter to human intuition. Being motivated by the observation, we propose a more robust 3D shape retrieval system which is called the irrelevance filtering and similarity ranking (IF/SR) method. Its retrieved results are shown in the second row of each subfigure. All mistakes generated by DG1SIFT are corrected by our method. Clearly, the proposed IF/SR system has a more robust performance as shown in these examples.

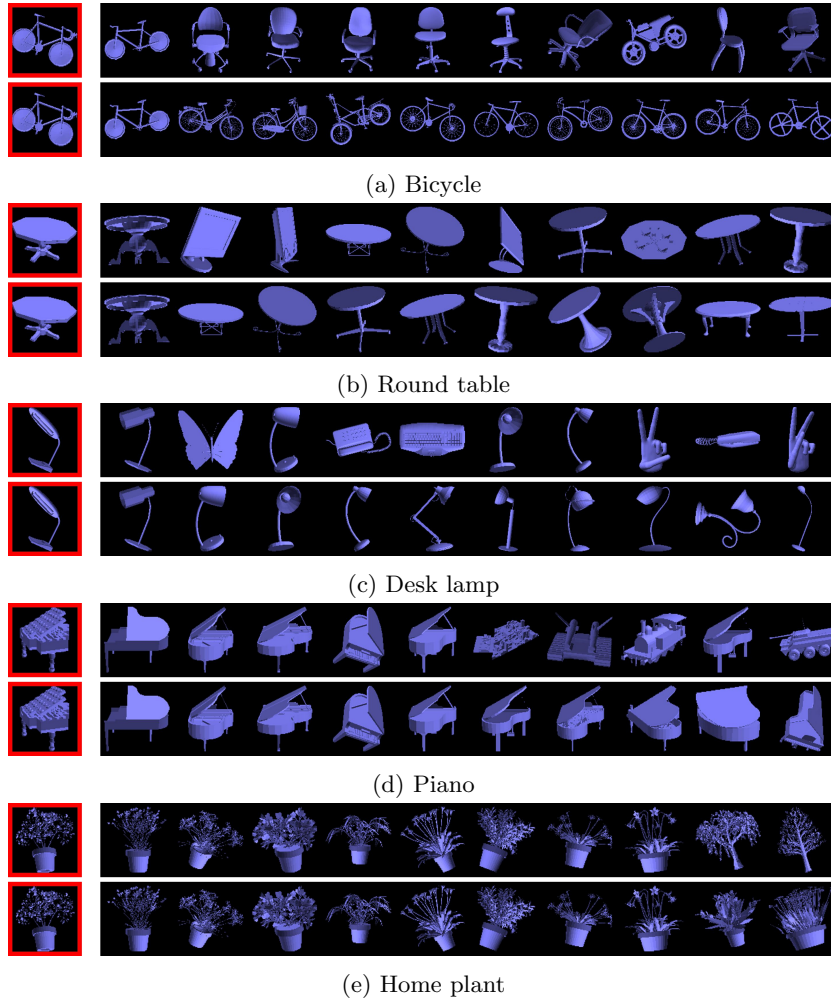


Fig. 1: Comparison of retrieved shapes using the DG1SIFT method (the first row) and the proposed IF/SR method (the second row) against five query shapes (from top to bottom): (a) bicycle, (b) round table, (c) desk lamp, (d) piano, and (e) home plant.

There are two main contributions of this work. First, we develop more powerful and robust global features to compensate for the weaknesses of local features. Feature concatenation are often adopted by traditional methods to combine local and global features. However, proper feature weighting and dimension reduction remain to be a problem. For the second contribution, we propose a robust shape retrieval system that consists of two modules in cascade: the irrelevance filtering (IF) module and the similarity ranking (SR) module. The IF module attempts

to cluster gallery shapes that are similar to each other by examining global and local features simultaneously. However, shapes that are close in the local feature space can be distant in the global feature space, and vice versa. To resolve this issue, we propose a joint cost function that strikes a balance between two distances. In particular, irrelevant samples that are close in the local feature space but distant in the global feature space can be removed in this stage. The remaining gallery samples are ranked in the SR module using the local feature.

The rest of this paper is organized as follows. The proposed IF/SR method is explained in Section 2. Experimental results are shown in Section 3. Finally, concluding remarks are given in Section 4.

2 Proposed IF/SR Method

2.1 System Overview

The flow chart of the proposed IF/SR method is shown in Fig. 2. The IF module is trained in an off-line process with the following three steps.

1. **Initial label prediction.** All gallery samples are assigned an initial label in their local feature space using an unsupervised clustering method.
2. **Local-to-global feature association.** Samples close to each cluster centroid are selected as the training data. A random forest classifier is trained based on their global features. All gallery samples are re-predicted by the random forest classifier to build an association from the local feature space to the global feature space.
3. **Label refinement.** We assign every gallery sample a set of relevant cluster indices based on a joint cost function. The joint cost function consists of two assignment scores. One score reflects the relevant cluster distribution of the query sample itself while the other is the mean of the relevant cluster distributions of its local neighbors. The ultimate relevant cluster indices are obtained by thresholding the cost function.

In the on-line query process, we extract both global and local features from a query shape and proceed with the following two steps.

1. **Relevance prediction.** we adopt the same scheme in the label refinement step to assign relevant cluster indices to a given query.
2. **Similarity ranking.** The similarity between the query and all relevant gallery samples is measured in the local feature space. In this step, a post-processing technique can also be adopted to enhance retrieval accuracy.

An exemplary query, desk lamp, is given in Fig. 2 to illustrate the on-line retrieval process. In the dashed box “retrieval without Stage I”, the traditional local feature (DG1SIFT) retrieves erroneous shapes such as butterfly, desk phone and keyboard in the top five ranks. They are apparently irrelevant to the query

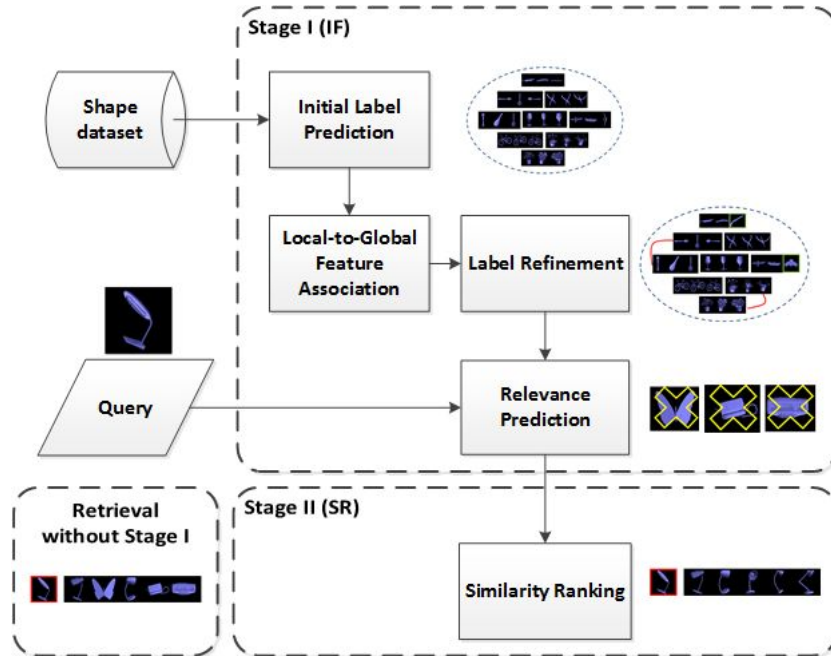


Fig. 2: The flow chart of the proposed IF/SR system.

shape and successfully removed in the relevance prediction step in the IF stage (Stage I). The retrieved top five samples in the SR stage (Stage II) are all desk lamp shapes. We will explain the processing of Stages I and II in detail below.

2.2 Stage I: Irrelevance Filtering

3D Shape Preprocessing. We have two preprocessing steps: 1) model representation conversion and 2) 3D shape normalization. For model representation conversion, since we extract features from both mesh models and volumetric models, we adopt the parity count method [29] to convert a mesh model into a volumetric model. Each volumetric model has resolution $256 \times 256 \times 256$. 3D shape normalization aims to align shapes of the same class consistently to achieve translational, scaling and rotational invariance.

Translational invariance is achieved by aligning the center of mass with the origin. For scale invariance, we re-scale a shape to fit a unit sphere. For rotational invariance, we adopt the reflective symmetry axial descriptor [30] to calculate the nearly complete symmetry function for each 3D shape. The PCA on the symmetry function extracts three principal axes to form three principal planes. To determine the order of three principal planes, we project the shape into each plane and the projection views with the first and second largest areas are aligned with the XOY plane and the ZOY plane, respectively. Finally, the YOZ plane

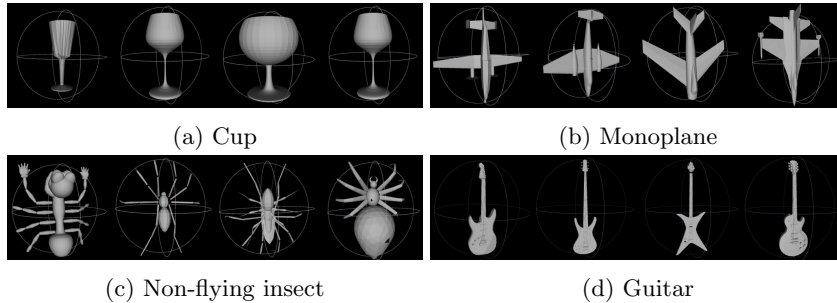


Fig. 3: Shape normalization results of four 3D shape classes.

is determined automatically. Fig. 3 shows some normalization results using the above-mentioned method.

Global Features. To capture the global properties of a 3D shape, we describe it using three feature types: 1) surface features (f_s), 2) wavelet features (f_w) and 3) geometrical features (f_g).

The 3D surface features, denoted by f_s , are a generalization of the 2D polar Fourier descriptor [31]. N rays are emitted from the origin of a normalized 3D shape. Each ray has the orientation $\mathbf{r} = (\cos\phi\cos\theta, \cos\phi\sin\theta, \sin\phi)$ with two directional parameters (θ, ϕ) , where θ and ϕ are uniformly sampled from intervals $[0, \pi)$ and $[0, 2\pi)$, respectively, with step size $\frac{\pi}{6}$. For each ray, the Euclidean distance from the origin to its intersected point on a face forms a function $g(\theta, \phi)$. If a ray intersects with multiple faces, we consider the farthest one only. In this way, we convert the original surface function $f(x, y, z)$ into a 2D distance function parameterized by $g(\theta, \phi)$. Then, we calculate the Fourier coefficients of the 2D distance function. The magnitude information forms a 72-D feature vector denoted by f_s . The Fourier descriptors of four shapes belonging to two classes are visualized in Fig. 4, where each subfigure contains an original shape in the left and its surface feature in the right. We see intra-class consistency and inter-class discrimination from this figure.

For the wavelet features denoted by f_w , we adopt the generalized 3D Haar-like filters [32]. Seven bands of 3D Haar-like filters as shown in Fig. 5 are applied to a normalized and voxelized model. The first three filters capture the left-right, top-bottom, front-back symmetry properties. The last four filters analyze diagonal sub-regions. The responses from these seven filters form a 7D wavelet feature vector.

Furthermore, we incorporate four geometrical features: 1) the aspect ratio, 2) xyz-invariance, 3) $\alpha\beta\gamma$ -invariance and 4) rectilinearity[33]. The aspect ratio is a 3D feature based on three side lengths - l_x, l_y, l_z of the bounding box of a normalized shape. It is expressed as

$$AR = \left[\frac{l_x}{l_x + l_y + l_z}, \frac{l_y}{l_x + l_y + l_z}, \frac{l_z}{l_x + l_y + l_z} \right]. \quad (1)$$

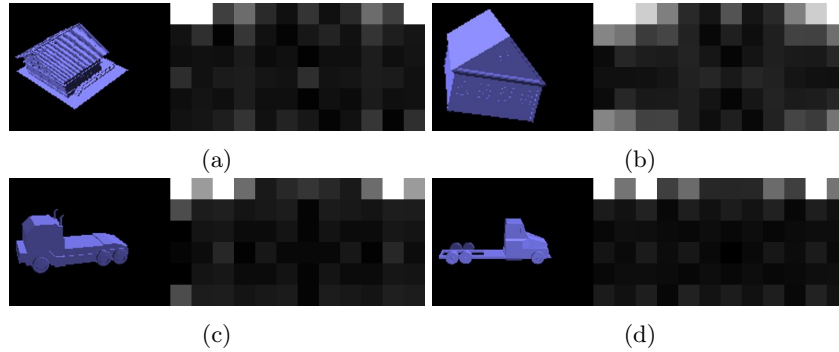


Fig. 4: Visualization of surface features of four shapes, where (a) and (b) provide two house shapes while (c) and (d) provide two truck shapes.

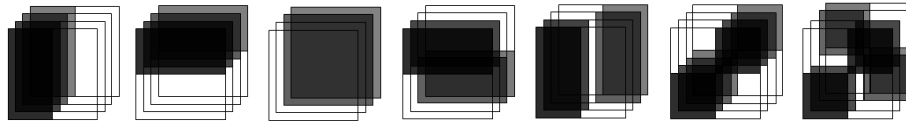


Fig. 5: Illustration of the seven-band Haar filters.

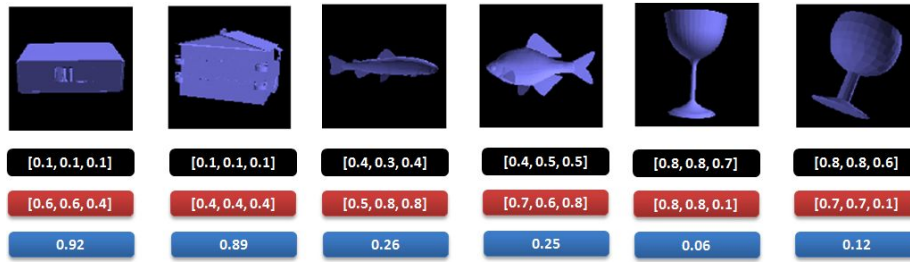


Fig. 6: The xyz-invariance (black box), $\alpha\beta\gamma$ -variance (red box) and rectilinearity (blue box) values of six examples from three classes: apartment house, fish and cup.

The xyz-variance and $\alpha\beta\gamma$ -variance are adopted to examine the variance of cut-planes of a normalized volumetric model. To measure the xyz-variance, we extract all cut-planes orthogonal to the X-axis, the Y-axis and the Z-axis, respectively. The variances of three groups of cut-planes form a 3D feature. Similarly, the $\alpha\beta\gamma$ -variance measures the variance of groups of rotated cut-planes centered at the X-axis, the Y-axis and the Z-axis, respectively. The robust rectilinearity measure from [33] is used to obtain the rectilinearity feature. It calculates the ratio between the total surface area and the sum of projected triangle areas on the XOY, the ZOY and the YOZ planes. Finally, the geometrical feature, denoted by f_g , is a 10-D feature vector. The geometrical features of six examples are

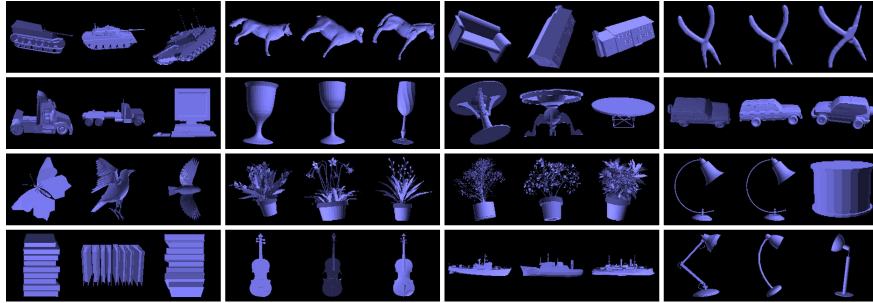


Fig. 7: Several clustered SHREC12 shapes using the spectral clustering method using the DG1SIFT feature.

shown in Fig. 6 in boxes of black (xyz -invariance), red ($\alpha\beta\gamma$ -variance) and blue (rectilinearity), respectively.

Initial Label Prediction. In traditional 3D shape retrieval formulation, all shapes in the dataset are not labeled. Under this extreme case, we select the spectral clustering algorithm [34] to reveal the underlying relationship between gallery samples. The local feature is strong at grouping locally similar shapes but it is sensitive to local variances as discussed in Section 1. In contrast, the global feature is powerful at differentiating global dissimilar shapes but weak at finding locally similar shapes. Thus, the combination of the two in this early stage tends to cause confusion and lower the performance. For this reason, we use the local feature only to perform clustering.

For the SHREC12 dataset, shapes in several clusters using the DG1SIFT feature are shown in Fig. 7. Some clusters look reasonable while others do not. Actually, any unsupervised clustering method will encounter two challenges. First, uncertainty occurs near cluster boundaries so that samples near boundaries have a higher probability of being wrongly clustered. Second, the total number of shape classes is unknown. When the cluster number is larger than the class number in the database, the clustering algorithm creates sub-classes or even mixed classes. We address the first challenge in the local-to-global feature association step and the second challenge in the label refinement step.

Local-to-Global Feature Association. We extract N_k samples closest to the centroid of the k^{th} cluster and assign them a cluster label. Clearly, samples sharing the same cluster label are close to each other in the feature space. There is a trade-off in choosing a proper value of N_k . A smaller N_k guarantees higher clustering accuracy but fewer gallery samples will be assigned cluster labels. Empirically, we set the value of N_k to one half of the size of the k^{th} cluster. Then, we convert the gallery samples from the local feature space to a global feature space. We will correct clustering errors in the global feature space at a later stage. Furthermore, samples that come from the same class but are separated in the local feature space can be merged by their global features. To build the association, labeled samples are used to train a random forest classifier [35]

with global features. Finally, all gallery shapes are treated as test samples. The random forest classifier is used to predict the probability of each cluster type by voting. In this way, samples clustered in the local feature space can be linked to multiple clusters probabilistically due to the similarity in the global feature space.

Label Refinement. The output of the IF module includes: 1) a set of indexed clusters, and 2) soft classification (or multi-labeling) of all gallery samples. For item #1, we use unsupervised spectral clustering to generate clusters as described above. If the class number is known (or can be estimated), it is desired that the cluster number is larger than the class number. Each of these clusters is indexed by a cluster ID. For item #2, we adopt soft classification so that each sample can be associated with multiple clusters. This is done for two reasons. If two sub-classes belong to the same ground truth class, we need a mechanism to re-group them together. Clearly, a hard classification process does not allow this to happen. Second, a hard classification error cannot be easily compensated while a soft classification error is not as fatal and it is likely to be fixed in the SR module (stage II).

We consider two relevant cluster assignment schemes below.

1) *Direct Assignment*

We apply the random forest classifier to both training and testing samples based on their global features. Then, the probability for the i^{th} shape sample (denoted by y_i) belonging to the k^{th} cluster (denoted by c_k) can be estimated by the following normalized voting result:

$$P_{rf}(y_i \in c_k) = \frac{v_k}{\sum_j v_j}, \quad (2)$$

where v_k is the number of votes claiming that y_i belongs to c_k . Eq. (2) associates y_i to its relevant clusters directly.

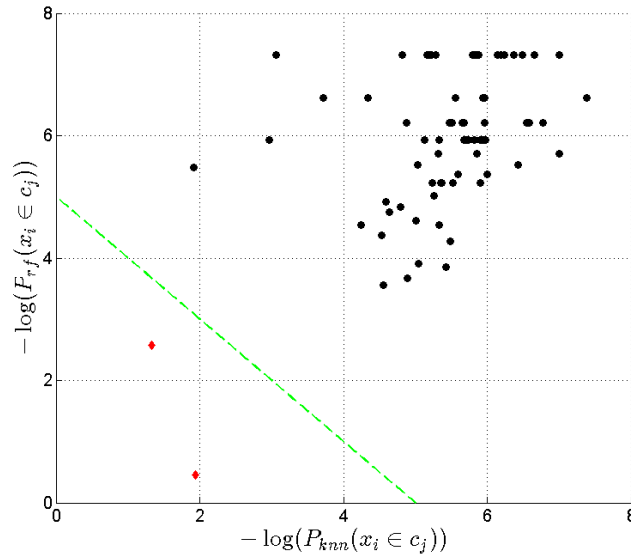
2) *Indirect Assignment*

Intuitively, a good cluster relevance assignment scheme should take both global and local features into account. For query sample, y_i , we find its K nearest neighbors (denoted by x_j) using a certain distance function in a local feature space (e.g. the same feature space used in DG1SIFT). Then, the probability of y_i belonging to c_k can be estimated by the weighted sum of the probability in Eq. (2) in form of

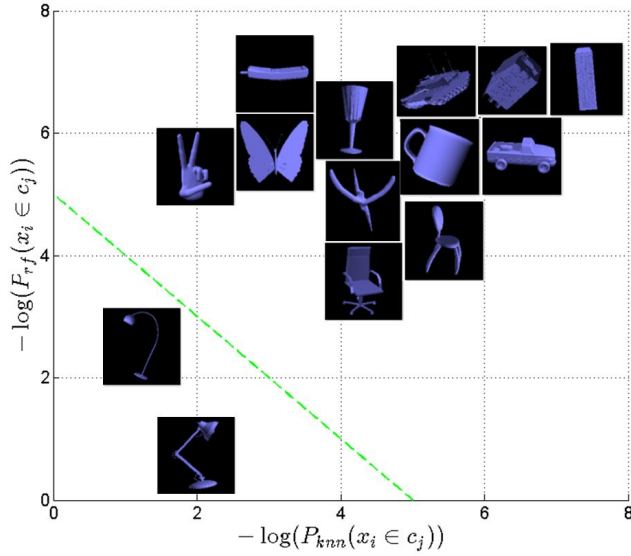
$$P_{knn}(y_i \in c_k) = \frac{\sum_{x_j \in knn(y_i)} P_{rf}(x_j \in c_k)}{\sum_{c_m} \sum_{x_j \in knn(y_i)} P_{rf}(x_j \in c_m)}. \quad (3)$$

Eq. (3) associates y_i to its relevant clusters indirectly. That is, the assignment is obtained by averaging the relevant clusters assignment of its K nearest neighbors. Empirically, we choose K to be 1.5 times the average cluster size in the experiments.

We show an example that assigns a query desk lamp shape to its relevant clusters in Fig. 8(a), whose x-axis and y-axis are the negative log functions of Eqs.



(a)



(b)

Fig. 8: Selecting relevant clusters for the query desk lamp in Fig. 1(c) by thresholding a cost function shown in Eq. 4.

(2) and (3), respectively. Every dot in Fig. 8(a) represents a cluster after shape clustering. To visualize shapes represented by a dot, we plot a representative sample of each cluster in Fig. 8(b).

We see that the distance between the hand cluster and the desk lamp cluster is small in the x-axis but large in the y-axis. This is because that samples of the desk lamp and hand clusters are interleaved in the local feature space as shown in the retrieval results of DG1SIFT in Fig. 1(c). However, the desk lamp and the hand clusters have little intersection in the global feature space. In contrast, the wheel chair and desk lamp clusters have large intersection in the global feature space. Yet, their distance is far in the local feature space. It is apparent that Eqs. (2) and (3) provide complementary relevance assignment strategies for query sample y_i . It is best to integrate the two into one assignment scheme. For example, we can draw a line to separate relevant and irrelevant clusters with respect to the query apple shape in this plot.

Mathematically, we can define the following cost function

$$\begin{aligned} \mathbb{J}(y_i, c_k) &= -\log(P_{knn}(y_i \in c_k)P_{rf}(y_i \in c_k)) \\ &= -[\log(P_{knn}(y_i \in c_k)) + \log(P_{rf}(y_i \in c_k))]. \end{aligned} \quad (4)$$

We compute $\mathbb{J}(y_i, c_k)$ for all clusters c_k . If

$$\mathbb{J}(y_i, c_k) < \epsilon, \quad (5)$$

where ϵ is a pre-selected threshold. We say that cluster c_k is a relevant cluster for query y_i . Otherwise, it is irrelevant.

2.3 Stage II: Similarity Ranking

In the SR module, we rank the similarity between a given query and gallery samples in the retrieved relevant clusters using a local-features-based matching scheme (e.g., DG1SIFT). Additionally, we adopt the Local Constrained Diffusion Process (LCDP) [36] in the post-processing step. The diffusion process is slightly modified with the availability of relevant clusters in the IF/SR system since the diffusion process can be conducted on a more reasonable manifold due to the processing in Stage I.

3 Experimental Results

We demonstrate the retrieval performance of the proposed IF/SR method by conducting experiments on the generic 3D shape dataset of SHREC12 [10]. It contains 1200 3D shapes in 60 independent classes. Samples are uniformly distributed so that each class has 20 shape samples. The retrieval performance is measured by five standard metrics. They are: Nearest-Neighbor (NN), First-Tier score (FT), Second-Tier score (ST), E-measurement (E), Discounted Cumulative Gain (DCG).

We compare the proposed IF/SR method with five state-of-the-art methods:

- LSD-sum [37]. It uses a local surface-based feature that considers local geodesic distance distribution and Bag-of-Words.

Table 1: Comparison of the First-Tier (FT) scores with different cluster numbers for the IF/SR method in the SHREC12 dataset. The best score is shown in bold.

M	16	32	48	64	80	96	112
FT	0.666	0.672	0.709	0.720	0.717	0.717	0.715

Table 2: Comparison of the NN, FT, ST, E and DCG scores of five state-of-the-art methods, the proposed IF/SR method, and the IF/SR method with LCDP postprocessing for the SHREC12 dataset. The best score for each measurement is shown in bold.

Method	NN	FT	ST	E	DCG
LSD-sum	0.517	0.232	0.327	0.224	0.565
ZFDR	0.818	0.491	0.621	0.442	0.776
3DSP_L2_1000_chi2	0.662	0.367	0.496	0.346	0.678
DVD+DB+GMR	0.828	0.613	0.739	0.527	0.833
DG1SIFT	0.879	0.661	0.799	0.576	0.871
IF/SR	0.896	0.720	0.837	0.608	0.891
IF/SR+LCDP	0.893	0.734	0.858	0.620	0.899

- ZFDR [38]. It adopts a hybrid feature that integrates the Zernike moment, the Fourier descriptor, the ray-based features.
- 3DSP_L2_1000_chi2 [10]. It employs a local surface-based feature that computes the 3D SURF descriptor under the spatial pyramid matching scheme.
- DVD+DB+GMR [10]. It adopts a hybrid feature that contains a dense voxel spectrum descriptor and a depth-buffer shape descriptor.
- DG1SIFT [24]. It uses a view-based feature that extracts three types of SIFT features (Dense SIFT, Grid SIFT and One SIFT) per view.

The IF/SR method adopts DG1SIFT as the local feature for shape clustering. We show the first-tier (FT) scores of the IF/SR method using a different cluster number M for shape clustering in Table 1. Generally speaking, the performance degrades when M is small due to the loss of discriminability in larger cluster sizes. The retrieval performance improves as the cluster number increases up to 64. After that, the performance saturates and could even drop slightly. That means that we lose the advantage of clustering when the cluster size is too small. For the remaining experimental results, we choose $M = 64$.

We compare the performance of seven 3D shape retrieval methods with five measures in Table 2. Clearly, the proposed IF/SR method (with or without LCDP postprocessing) outperforms the other five benchmarking methods. The IF/SR method with postprocessing improves the result of DG1SIFT by around 7% in the First-Tier score. Since DG1SIFT adopts the manifold ranking process in its similarity measurement, the gap between the IF/SR method before and after LCDP is relatively small.

Table 3: Comparison of top 20, 25, 30, 35, 40 retrieval accuracy for the SHREC12 dataset, where the best results are shown in bold.

N	20	25	30	35	40
LSD-sum	0.232	0.260	0.286	0.310	0.327
ZFDR	0.491	0.539	0.575	0.603	0.621
3DSP_L2_1000_chi2	0.367	0.411	0.446	0.476	0.496
DVD+DB+GMR	0.613	0.656	0.691	0.719	0.739
DG1SIFT	0.661	0.718	0.756	0.783	0.799
IF/SR	0.720	0.775	0.802	0.824	0.837
IF/SR+LCDP	0.734	0.786	0.817	0.841	0.858

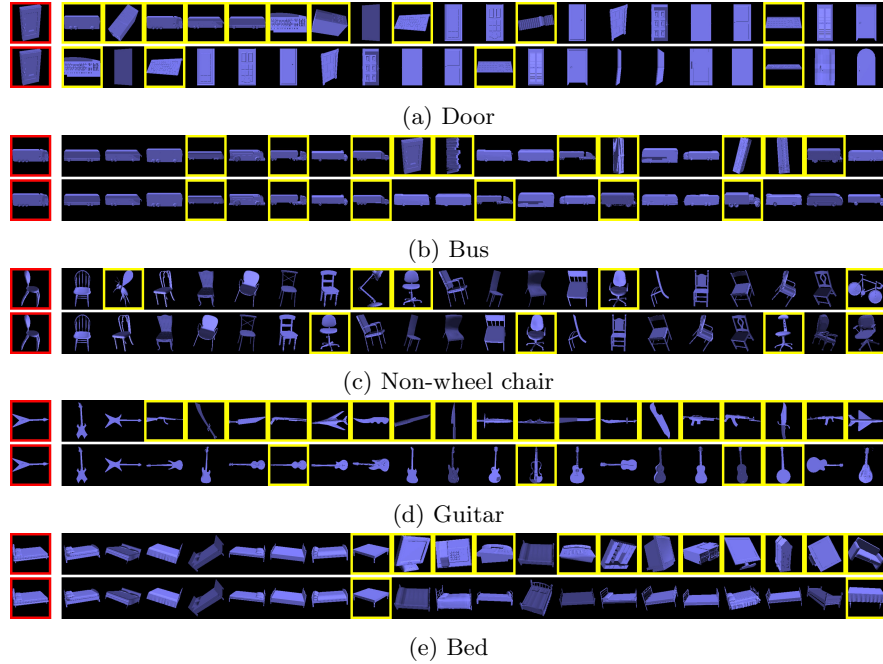


Fig. 9: Comparison of retrieved top 20 rank-ordered shapes. For each query case given in the leftmost column, retrieved results of DG1SIFT and the proposed IF/SR method are shown in the first and second rows of all subfigures, respectively.

Since each SHREC12 shape class contains 20 shape samples, the measure of correctly retrieved samples from the top 20 (FT) and 40 (ST) ranks cannot reflect the true power of the proposed IF/SR method. To push the retrieval performance further, we compare the accuracy of retrieved results from the top 20, 25, 30, 35 and 40 ranks of the IF/SR method and five benchmarking methods in Table 3,

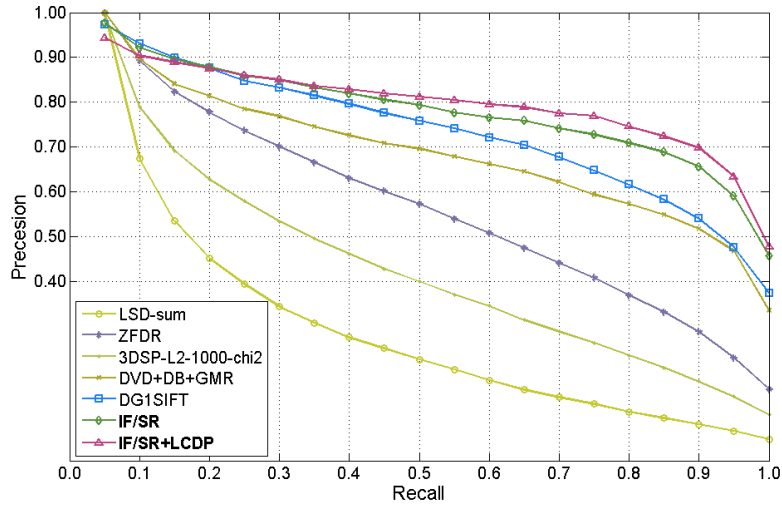


Fig. 10: Comparison of precision and recall curves of the proposed IF/SR method and several benchmarking methods for the SHREC12 dataset.

whose first and last columns correspond the FT and ST scores reported in Table 2. The superiority of the IF/SR method stands out clearly in this table.

According to the top 20 retrieval performance, the IF/SR method still makes mistakes for some queries. We conduct error analysis and show the results of DG1SIFT and the IF/SR method in Figs. 9(a)-(e). For each query case given in the leftmost column, retrieved results of DG1SIFT and the IF/SR method are shown in the first and second rows of all subfigures, respectively. Each erroneous result is enclosed by a thick frame. The errors of DG1SIFT are obvious. They are far away from human experience. The IF/SR method makes mistakes between door/keyboard, bus/truck, non-wheel chair/wheel chair, guitar/violin and bed/rectangle table (see the second row of all subfigures). These mistakes are more excusable since they are closer to each other based on human judgment.

Finally, we show the precision-and-recall curves of the IF/SR method and several methods in Fig. 10. We see from the figure that the IF/SR method outperforms all other methods by a significant margin.

4 Conclusion

The IR/SF method was proposed to solve the unsupervised 3D shape retrieval problem. In the IF stage, irrelevant shape clusters are removed for each query shape. In the SR stage, the system can focus on the matching and ranking in a much smaller subset of shapes. Its superior retrieval performance was evaluated on the popular SHREC12 dataset.

References

1. Tangelder, J.W., Veltkamp, R.C.: A survey of content based 3d shape retrieval methods. *Multimedia tools and applications* **39** (2008) 441–471
2. Su, H., Maji, S., Kalogerakis, E., Learned-Miller, E.: Multi-view convolutional neural networks for 3d shape recognition. In: *Proceedings of the IEEE International Conference on Computer Vision*. (2015) 945–953
3. Xie, J., Fang, Y., Zhu, F., Wong, E.: Deepshape: Deep learned shape descriptor for 3d shape matching and retrieval. In: *Proceedings of the IEEE Conference on Computer Vision and Pattern Recognition*. (2015) 1275–1283
4. Shi, B., Bai, S., Zhou, Z., Bai, X.: Deeppano: Deep panoramic representation for 3-d shape recognition. *IEEE Signal Processing Letters* **22** (2015) 2339–2343
5. Savva, M., Yu, F., Su, H., Aono, M., Chen, B., Cohen-Or, D., Deng, W., Su, H., Bai, S., Bai, X., et al.: (Shrec16 track large-scale 3d shape retrieval from shapenet core55)
6. Bai, S., Bai, X., Zhou, Z., Zhang, Z., Jan Latecki, L.: Gift: A real-time and scalable 3d shape search engine. In: *The IEEE Conference on Computer Vision and Pattern Recognition (CVPR)*. (2016)
7. Wu, Z., Song, S., Khosla, A., Yu, F., Zhang, L., Tang, X., Xiao, J.: 3d shapenets: A deep representation for volumetric shapes. In: *Proceedings of the IEEE Conference on Computer Vision and Pattern Recognition*. (2015) 1912–1920
8. Maturana, D., Scherer, S.: Voxnet: A 3d convolutional neural network for real-time object recognition. In: *Intelligent Robots and Systems (IROS), 2015 IEEE/RSJ International Conference on, IEEE* (2015) 922–928
9. Qi, C.R., Su, H., Niessner, M., Dai, A., Yan, M., Guibas, L.J.: Volumetric and multi-view cnns for object classification on 3d data. *arXiv preprint arXiv:1604.03265* (2016)
10. Li, B., Godil, A., Aono, M., Bai, X., Furuya, T., Li, L., López-Sastre, R.J., Johan, H., Ohbuchi, R., Redondo-Cabrera, C., et al.: Shrec’12 track: Generic 3d shape retrieval. In: *3DOR*. (2012) 119–126
11. Kazhdan, M., Funkhouser, T., Rusinkiewicz, S.: Rotation invariant spherical harmonic representation of 3 d shape descriptors. In: *Symposium on geometry processing*. Volume 6. (2003) 156–164
12. Osada, R., Funkhouser, T., Chazelle, B., Dobkin, D.: Shape distributions. *ACM Transactions on Graphics (TOG)* **21** (2002) 807–832
13. Smeets, D., Keustermans, J., Vandermeulen, D., Suetens, P.: meshsift: Local surface features for 3d face recognition under expression variations and partial data. *Computer Vision and Image Understanding* **117** (2013) 158–169
14. Bronstein, M.M., Kokkinos, I.: Scale-invariant heat kernel signatures for non-rigid shape recognition. In: *Computer Vision and Pattern Recognition (CVPR), 2010 IEEE Conference on, IEEE* (2010) 1704–1711
15. Bronstein, A.M., Bronstein, M.M., Guibas, L.J., Ovsjanikov, M.: Shape google: Geometric words and expressions for invariant shape retrieval. *ACM Transactions on Graphics (TOG)* **30** (2011) 1
16. Gal, R., Shamir, A., Cohen-Or, D.: Pose-oblivious shape signature. *IEEE transactions on visualization and computer graphics* **13** (2007) 261–271
17. Reuter, M., Wolter, F.E., Peinecke, N.: Laplace–beltrami spectra as shape-dnaof surfaces and solids. *Computer-Aided Design* **38** (2006) 342–366
18. Lian, Z., Godil, A., Bustos, B., Daoudi, M., Hermans, J., Kawamura, S., Kurita, Y., Lavoua, G., Dp Suetens, P.: Shape retrieval on non-rigid 3d watertight meshes. In: *Eurographics Workshop on 3D Object Retrieval (3DOR)*. (2011)

19. Lian, Z., Zhang, J., Choi, S., ElNaghy, H., El-Sana, J., Furuya, T., Giachetti, A., Guler, R., Isaia, L., Lai, L., et al.: Shrec15 track: Non-rigid 3d shape retrieval. In: Proc Eurographics Workshop on 3D Object Retrieval. (2015)
20. Chen, D.Y., Tian, X.P., Shen, Y.T., Ouhyoung, M.: On visual similarity based 3d model retrieval. In: Computer graphics forum. Volume 22., Wiley Online Library (2003) 223–232
21. Chaouch, M., Verroust-Blondet, A.: A new descriptor for 2d depth image indexing and 3d model retrieval. In: Image Processing, 2007. ICIP 2007. IEEE International Conference on. Volume 6., IEEE (2007) VI–373
22. Ohbuchi, R., Osada, K., Furuya, T., Banno, T.: Salient local visual features for shape-based 3d model retrieval. In: Shape Modeling and Applications, 2008. SMI 2008. IEEE International Conference on, IEEE (2008) 93–102
23. Lowe, D.G.: Object recognition from local scale-invariant features. In: Computer vision, 1999. The proceedings of the seventh IEEE international conference on. Volume 2., Ieee (1999) 1150–1157
24. Ohbuchi, R., Furuya, T.: Distance metric learning and feature combination for shape-based 3d model retrieval. In: Proceedings of the ACM workshop on 3D object retrieval, ACM (2010) 63–68
25. Li, B., Lu, Y., Li, C., Godil, A., Schreck, T., Aono, M., Chen, Q., Chowdhury, N.K., Fang, B., Furuya, T., et al.: Shrec14 track: Large scale comprehensive 3d shape retrieval. In: Eurographics Workshop on 3D Object Retrieval. Volume 2014. (2014) 131–40
26. Bronstein, A., Bronstein, M., Castellani, U., Dubrovina, A., Guibas, L., Horaud, R., Kimmel, R., Knossow, D., Von Lavante, E., Mateus, D., et al.: Shrec'10 track: correspondence finding. In: 3DOR2010-Eurographics Workshop on 3D Object Retrieval, Eurographics Association (2010) 87–91
27. Dutagaci, H., Godil, A., Daras, P., Axenopoulos, A., Litos, G., Manolopoulou, S., Goto, K., Yanagimachi, T., Kurita, Y., Kawamura, S., et al.: Shrec'11 track: generic shape retrieval. In: Proceedings of the 4th Eurographics conference on 3D Object Retrieval, Eurographics Association (2011) 65–69
28. Li, B., Lu, Y., Li, C., Godil, A., Schreck, T., Aono, M., Burtscher, M., Chen, Q., Chowdhury, N.K., Fang, B., et al.: A comparison of 3d shape retrieval methods based on a large-scale benchmark supporting multimodal queries. *Computer Vision and Image Understanding* **131** (2015) 1–27
29. Nooruddin, F.S., Turk, G.: Simplification and repair of polygonal models using volumetric techniques. *Visualization and Computer Graphics, IEEE Transactions on* **9** (2003) 191–205
30. Kazhdan, M., Chazelle, B., Dobkin, D., Funkhouser, T., Rusinkiewicz, S.: A reflective symmetry descriptor for 3d models. *Algorithmica* **38** (2004) 201–225
31. Zhang, D., Lu, G.: An integrated approach to shape based image retrieval. In: Proceedings of 5th Asian Conference on Computer Vision (ACCV), Melbourne, Australia. (2002)
32. Cui, X., Liu, Y., Shan, S., Chen, X., Gao, W.: 3d haar-like features for pedestrian detection. In: Multimedia and Expo, 2007 IEEE International Conference on, IEEE (2007) 1263–1266
33. Lian, Z., Rosin, P.L., Sun, X.: Rectilinearity of 3d meshes. *International Journal of Computer Vision* **89** (2010) 130–151
34. Ng, A.Y., Jordan, M.I., Weiss, Y., et al.: On spectral clustering: Analysis and an algorithm. *Advances in neural information processing systems* **2** (2002) 849–856
35. Breiman, L.: Random forests. *Machine learning* **45** (2001) 5–32

36. Yang, X., Koknar-Tezel, S., Latecki, L.J.: Locally constrained diffusion process on locally densified distance spaces with applications to shape retrieval. In: Computer Vision and Pattern Recognition, 2009. CVPR 2009. IEEE Conference on, IEEE (2009) 357–364
37. BAI, X., LI, L., ZHANG, S.: Software for 3d model retrieval using local shape distributions (2012)
38. Li, B., Johan, H.: 3d model retrieval using hybrid features and class information. *Multimedia tools and applications* **62** (2013) 821–846